CrossMark

Complementary Studies of Phase Formation During Fabrication of $Fe_{0.65}Co_{0.35}$ Nanoparticles by Mechanical Alloying

DO HUNG MANH ⬤,[1,5,6] D.K. TUNG,[1] L.T.H. PHONG,[1]
NGUYEN XUAN PHUC,[1,2] P.T. PHONG,[3] JARU JUTIMOOSIK,[4]
and RATTIKORN YIMNIRUN[4]

1.—Institute of Materials Science, Vietnam Academy of Science and Technology, 18 Hoang Quoc Viet Road, Cau Giay District, Hanoi, Vietnam. 2.—Duy Tan University, K7/25 Quang Trung, Da Nang, Vietnam. 3.—Khanh Hoa University, Nha Trang, Vietnam. 4.—Institute of Science and NANOTEC-SUT COE on Advanced Functional Nanomaterials, School of Physics, Suranaree University of Technology, Nakhon Ratchasima, Thailand. 5.—e-mail: manhdh.ims@gmail.com. 6.—e-mail: manhdh@ims.vast.ac.vn

Fe-Co nanoparticles were prepared by mechanical alloying in air with various milling times from 0 h to 10 h and annealing temperatures in the range from 773 K to 973 K. The combined use of both conventional x-ray diffraction (XRD) and synchrotron x-ray absorption spectroscopy (XAS) techniques allowed us to obtain accurate data on the phase formation and the oxidation state of the materials. XRD patterns reveal a secondary phase of Fe_3O_4 that is present in as-milled samples and those annealed in Ar + H_2 (5%) at temperatures of up to 600°C. This secondary phase disappeared for annealing temperatures of over 700°C. Meanwhile, analyses of Fe K-edge x-ray absorption near-edge structure (XANES) and extended x-ray absorption fine structure (EXAFS) spectra clearly showed that the local structure around Fe of all samples were of a bcc structure and had the oxidation state of +0. Most importantly, the ratio of bcc and hcp structures was also extracted from the Co K-edge XANES and the measured K-weighted EXAFS spectra of the alloyed Fe-Co samples. Moreover, magnetization measurements at room temperature indicated that the saturation magnetization (M_s) increased with increasing milling time and annealing temperature. While the former behavior is assigned to the Fe-Co alloy formation, we believe the effects of reducing the oxidation of the annealed samples to be the major cause of the enhanced M_s. The dependence of coercivity (H_c) on milling time and annealing temperature was also investigated and discussed.

Key words: Fe-Co alloys, x-ray absorption spectroscopy, x-ray diffraction, magnetic property, oxidation

INTRODUCTION

Magnetic nanoparticles with high saturation magnetization are considered very important for exchange-coupled nanocomposite magnets, microwave absorbing, and biomedical applications.[1–5] Fe-Co alloy nanoparticles have been intensively investigated because of their high saturation magnetization and other remarkable magnetic properties, such as H_c, magnetic ordering temperature, and hyperfine magnetic field. These magnetic properties significantly differ from those of other microcrystalline materials and are highly sensitive to the structure and microstructure of a given material.[6–9]

Several techniques have been used to synthesize Fe-Co alloy powders, such as polyol, coprecipitation, electrochemistry, and ball milling.[6,10–13] Mechanical alloying (MA) is one of the most common and efficient methods to obtain nanocrystalline oxides

and alloys,[1,7,12,14] especially considering the large industrial scale of the applications. Fe-Co alloy nanoparticles obtained by MA are usually prepared by using Fe and Co powders under an argon atmosphere. The phase formation and magnetic properties of MA Fe-Co nanoparticles has been fully investigated and is now well understood.[7–9]

Recently, Fe-Co nanoparticles prepared by MA in air have been reported.[8,13,15,16] One issue that could arise from this technique is that the oxide phases of Fe and/or Co could be co-formed during the millings in air, however, we have detected the presence of only a small amount of the Fe_3O_4 phase (in the as-milled sample for 10 h) from the x-ray diffraction (XRD) pattern.[16] The effects of oxidation are interesting issues that require further investigation.

XRD and x-ray absorption spectroscopy (XAS) are powerful techniques used for investigating the structure of materials. XRD can be used to determine the formation of nanocrystalline phases and to gather information on average crystal size, while XAS gives information about the local structure surrounding an absorbing atom.[17] Both techniques can be combined on one synchrotron beam line to study samples in a single experiment, as reported by Ehrlich et al.[18] To the best of our knowledge, no publication has been reported on the local crystallographic structure of Fe-Co alloys prepared by MA in air.

In the present study, we report a detailed study of the structure of $Fe_{0.65}Co_{0.35}$ nanoparticles prepared by MA with various milling times and annealing temperatures. Our aim is to verify the presence of an Fe_3O_4 phase in the samples during fabrication by using an appropriate control for recording the XRD patterns. Additionally, we report new findings from synchrotron x-ray absorption measurements on the formation and ratios of the nanocrystalline phases, as well as the oxidation state of Fe or Co ions in the samples. Finally, the effects of milling time and annealing temperature on the magnetic properties of Fe-Co were investigated and discussed.

EXPERIMENTAL

Synthesis

Commercial Fe and Co powders with a particle size less than 100 μm were used to prepare $Fe_{65}Co_{35}$ nanoparticles by MA. The MA process was performed in air using the P6 planetary ball miller with a ball-to-powder weight ratio of 15:1, a milling speed of 450 rpm, and a milling time (t_m) of 2–10 h. The M_s of the samples increased with milling time and reached a peak value (200 emu/g) after 10 h of milling, due to the progress of the alloying reaction between elemental Fe and Co powders (see Ref. 16 for more details). A small amount of powder that was milled for 10 h was used for thermal treatment processing. The samples were annealed for 1 h under flowing Ar + H_2 (5%) gas at different temperatures. Samples are labeled S1, S2, S3, S4, and S5

for the samples that were milled for 2, 4, 6, 8, and 10 h, and S6, S7, S8 for samples that were annealed at 773 K, 873 K, and 973 K, respectively.

Characterization Techniques

XRD data were collected with an x-ray diffractometer (Bruker, D8 ADVANCE with DAVINCI.-DESIGN, Cu-K_α radiation, $\lambda = 0.154$ nm) to determine the structural characterization of each sample. Diffraction patterns were recorded in a 2θ-angle range from 20º to 90° with a step size of 0.001°/s. The average crystallite size (D) and strain (σ) were determined by a Rietveld method using the commercial X-Pert HighScore with the Plus option program.

To distinguish different structures and oxidation states of Fe or Co ions in each samples, x-ray absorption near-edge structure (XANES) and extended x-ray absorption fine structure (EXAFS) spectra for all samples and reference compounds were acquired in transmission mode at Beamline 5.2 (SUT-NANOTEC-SLRI) of the Synchrotron Light Research Institute (SLRI), Nakhon Ratchasima, Thailand. A Ge (220) double crystal monochromator with an energy resolution ($\Delta E/E$) of 3×10^{-4} was used to scan the synchrotron x-ray beam. The normalized XANES and EXAFS data were processed after background subtraction in the pre-edge and post-edge region using ATHENA software, which is included in an IFEFFIT package.[19]

M_s and H_c of each sample were determined at room temperature using a homemade vibrating sample magnetometer (VSM) under externally applied magnetic fields of up to 12 kOe.

RESULTS AND DISCUSSION

XRD Analyses

Figure 1a shows a series of XRD patterns indicating the phase evolution with different milling times. As shown by this figure, when the milling time is less than 2 h, the Fe and Co diffraction peaks can be distinguished, but after 6 h of milling, the hcp Co peaks disappeared. The diffusion of Co into the Fe matrix leads to the formation of a disordered bcc Fe-Co solid solution.[8,20] For samples milled for 10 h, we observed strong and sharp diffraction peaks matching with bcc Fe-Co; we also observed weak diffraction peaks for the fcc phase of Fe_3O_4, but no traces of Co oxide were evidenced. These results are consistent with our previous report, in which the diffraction patterns were recorded under similar experimental conditions (very slow scanning rate of 0.001°/s).[13] In other words, the Fe_3O_4 phase could be found in $Fe_{65}Co_{35}$ powders prepared by MA in air by choosing an appropriate scanning rate for recording XRD patterns. In addition, the characteristic diffraction peaks of the fcc Fe-Co phase were broadened

Complementary Studies of Phase Formation During Fabrication of $Fe_{0.65}Co_{0.35}$ Nanoparticles by Mechanical Alloying

2503

gradually, while the intensity decreased with milling time. This behavior could be related to the decrease of crystallite size and an increase of internal strain during milling.[8,12,20]

Figure 1b presents XRD patterns of sample S5 and samples annealed at different temperatures, i.e., samples S6, S7, and S8. It clearly shows that the characteristic peaks for the bcc Fe_3O_4 phase diminish gradually as the annealing temperature
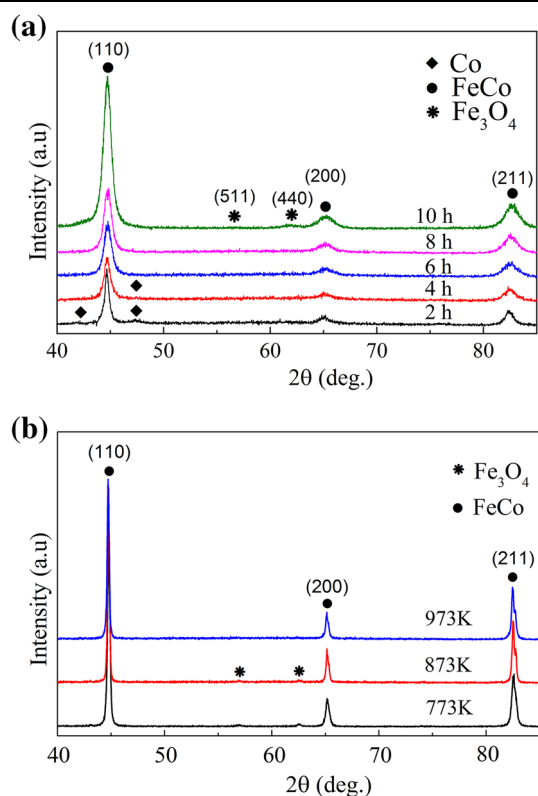

Fig. 1. XRD patterns of (a) Fe-Co powders milled for various milling times and (b) 10-h, as-milled powders subsequently annealed at the different temperatures.

increases and completely vanish at 973 K. This means that the Fe_3O_4 phase was reduced by hydrogen. At the same time, the width of the characteristic diffraction peaks of the fcc Fe-Co phase decreases, while the intensity increases with annealing temperature. This behavior could be due to the growth of crystallite size and the relief of strain with increasing annealing temperature.[7,12]

The best Rietveld refinement of the XRD patterns for the samples was performed and fitted to determine average crystallite size and strain. The fitting results are summarized in Table I, indicating that the changes of the average crystallite size and the strain with the milling times and the annealing temperatures are consistent with ones reported in Refs. 7, 12, and 20.

XANES and EXAFS Analyses

The XANES spectra of pure Fe and Co foils can be used as models for bcc and hcp structures, respectively. Figure 2 shows the Fe and Co K-edge-normalized XANES spectra of reference standards, indicating the differences in main edge position (valence), shape of main edge peak, and shoulders (geometry of local environment).

Figure 3 presents the Fe and Co K-edge XANES and EXAFS spectra of the alloyed Fe-Co samples along with the foil Fe(bcc) and Co(hcp) reference standards. The measured Fe K-edge XANES and EXAFS spectra presented in Fig. 3a and b clearly show that the local structure around Fe of all samples is of a bcc structure and has the oxidation state of +0. In other words, our XAS data showed no evidence of the Fe_3O_4 phase that was detected by the XRD measurement (see Fig. 1). Such, XAS technique is not sensitive enough to detect low concentrations of the Fe_3O_4 phase.

Importantly, from Co K-edge XANES and EXAFS measurements shown in Fig. 3c and d, we found that the peak position moved from the Co(hcp) shell peak near 4.1 Å to the Fe(bcc) shell peak near 4.5 Å between 2 h and 6 h. At the same time, the peak at

Table I. The dependence of average crystallite size (D) and strain (σ) on milling time (t_m) and annealing temperature (T_a) for nanocrystalline alloy powders

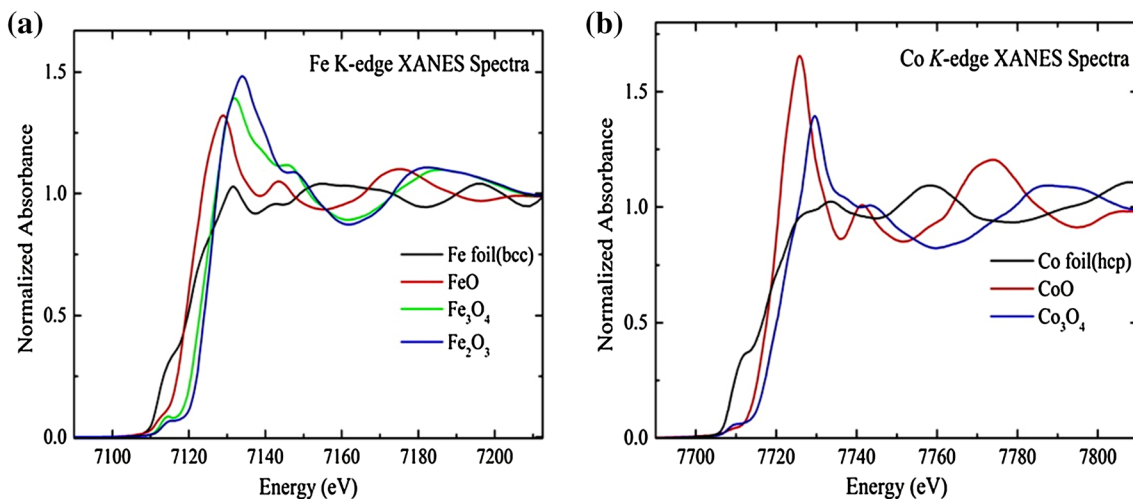| Sample name	Treatment		d (nm)	σ
	t_m (h)	T_a (K)		
S1	2		32(2)	0.185
S2	4		20(2)	0.316
S3	6		17(2)	0.337
S4	8		14(2)	0.363
S5	10		10(2)	0.380
S6	10	773	30(2)	na
S7	10	873	35(2)	na
S8	10	973	46(2)	na

na not available.

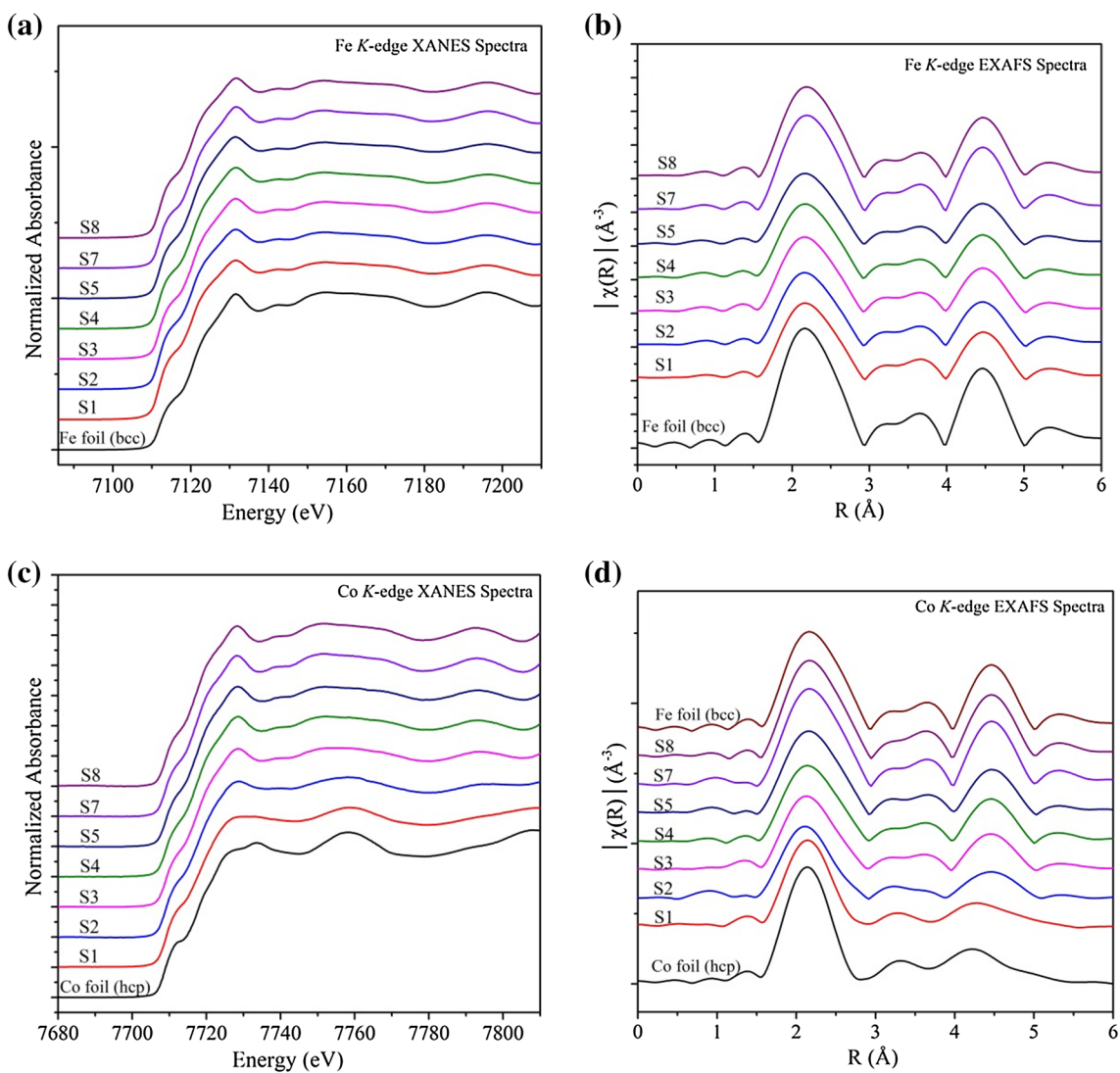Fig. 2. The normalized Fe and Co K-edge XANES spectra of (a) Fe and (b) Co standards.

Fig. 3. Comparison of the normalized XANES and the Fourier transforms of EXAFS spectra of (a, b) foil Fe(bcc)—obtained from Fe K-edge—and (c, d) foil Co(hcp)—obtained from Co K-edge—and the alloyed Fe-Co samples.

Complementary Studies of Phase Formation During Fabrication of $Fe_{0.65}Co_{0.35}$ Nanoparticles by Mechanical Alloying

2505

4.5 Å increased. This result is in agreement with those earlier reported in Ref. 21. In other words, the local structure of Co gradually changed from an hcp to a bcc structure when the alloying time was increased.

To better observe the transformation of Co from the hcp to bcc structure, Fig. 4 shows a plot of $k^2\chi(k)$ for the alloyed Fe-Co samples along with foils of Fe(bcc) and Co(hcp) reference standards, where k is the modulus of the wave vector of the photoelectron. As shown in Fig. 4, the peak position near 4.5 Å is similar to that of bcc Fe for all milled samples (6 h and 10 h), as well as annealed samples (773 K and 973 K). This result is consistent with observations from XRD patterns as shown in Fig. 1a.

Moreover, the proportion of bcc and hcp structures in the samples can be determined by using a linear combination fitting (LCF). In the LCF method, the x-ray absorption spectrum is modeled by least squares fitting using a linear combination of known species to fit an unknown spectrum. The LCF method can be applied to XANES, derivative XANES, or EXAFS spectra. The fitting results from the measured K-weighted EXAFS spectra of the alloyed Fe-Co samples are summarized in Table II. The fitting quality was also judged via the normalized sum of residuals (R-factor). From this table, it can be seen that the alloying process was incomplete for the sample that was milled for 10 h and was almost fulfilled after annealing at 973 K for 1 h.

In order to examine the fraction of Co in the hcp or bcc structure, we consider K-weighted EXAFS spectra of Fe(bcc) and Co(hcp) foils as the parent components for doing the LCF. The fit is done by generating the weighted sum of the two pure (bcc and hcp) signatures, i.e.,

$$S_{av}(k) = f_{bcc}S_{bcc}(k) + (1 - f_{bcc})S_{hcp}(k) \qquad (1)$$

where S_{bcc} and S_{hcp} are the measured bcc (Fe foil) and hcp (Co foil) EXAFS signature and f_{bcc} is a bcc fraction. f_{bcc} is allowed to vary between 1 (completely bcc structure) and 0 (completely hcp structure). The fitting results are shown in Table II.

In a similar way, we can determine the fraction of Co in bcc and hcp structures from the measured Co K-edge XANES spectra by using XANES spectra of S8 (completely bcc structure) and S1 (completely hcp structure) samples as parent components. The comparison of the normalized Fe K-edge XANES spectra of the alloyed Fe-Co samples and their fits using the LCF method is shown in Fig. 5. The proportions of two parent components obtained from the fitting also were shown in Table III. There are differences in the results given in Tables II and III due to sample S1 being regarded as having a completely hcp structure. However, the fitting results allow us to more accurately assess the alloying process during milling and annealing.
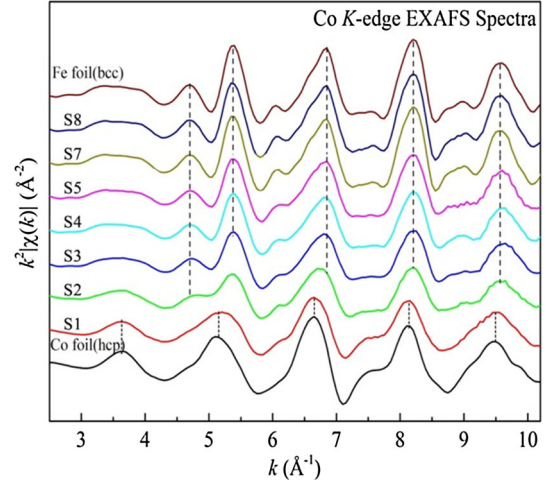

Fig. 4. Comparison of the measured K-weighted EXAFS spectra of Co foil(hcp), the alloyed Fe-Co samples and Fe foil(bcc).

Table II. The proportion of bcc and hcp structures extracted from the measured k-weighted EXAFS spectra of the alloyed Fe-Co samples

Samples	Proportion of bcc (Fe foil)	Proportion of hcp (Co foil)	R-factor
S1	0.212	0.788	0.0932
S2	0.551	0.449	0.2414
S3	0.740	0.260	0.1785
S4	0.831	0.169	0.1164
S5	0.835	0.165	0.0656
S7	0.936	0.064	0.0122
S8	0.961	0.039	0.0071

Magnetic Characterization

Figure 6a presents the variation of H_c of the samples as a function of milling time. It can be seen that the value of H_c decreases with milling time from 2 h to 4 h, then increases slightly for longer milling times. While the former behavior is attributed to the belief that there is a reduction of particle size, and could be explained based on a random anisotropy model;[22] the increase of H_c could be a consequence of several possibilities, e.g., internal strain (as shown in Table I), contamination, various defects, and/or particle interaction.[7] In other words, the behavior of the samples before annealing may also have an influence on H_c.

It can also be seen from Fig. 6b that the H_c of the samples after annealing was smaller than that of the as-milled sample. Additionally, we found that the tendency of H_c to change with the annealing temperatures of $Fe_{65}Co_{35}$ samples in this experiment is different than that our previous report in Ref. 23 but is similar to that of $Fe_{50}Co_{50}$ in Ref. 13. This may be due to the difference of the milling time
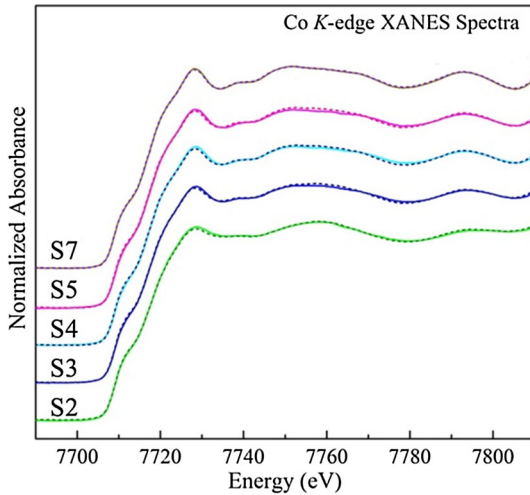
Fig. 5. Comparison of the normalized Fe K-edge XANES spectra of the alloyed Fe-Co samples (solid lines) and their fits (dash lines) using the LCF method.

Table III. The proportion of bcc and hcp structures extracted from the measured Co K-edge XANES spectra of the alloyed Fe-Co samples

Samples	Proportion of bcc (S8)	Proportion of hcp (S1)	R-factor
S2	0.405	0.595	0.00023
S3	0.672	0.328	0.00025
S4	0.836	0.164	0.00027
S5	0.822	0.178	0.00050
S7	0.994	0.006	0.00005

before annealing, which can produce alloy powders with different characteristics such as strain, defects, and oxidation.

Figure 7a presents the M_s dependence on milling time of the as-milled samples, showing the increase of the magnetization monotonically with the milling time. It is related to the progress of the alloying reaction between elemental Fe and Co powders during milling, as shown by XRD and XAS measurements presented earlier, as well as Mossbauer spectroscopy reported in Refs. 8, 9, and 24.

Figure 7b shows the changes of M_s for sample S5 annealed at different temperatures. The plot clearly shows that the M_s of all annealed samples was increased (compared to that of the sample S5). We believe that the enhancement of M_s is due to the reduction of the oxide phase (see Fig. 1b) as well as the growth of the particle size (see Table I). This result is consistent with a recent report.[16] However, it can also be seen from Fig. 7b that the M_s of all of the annealed samples is smaller overall than that of their bulk counterparts. This may be caused by
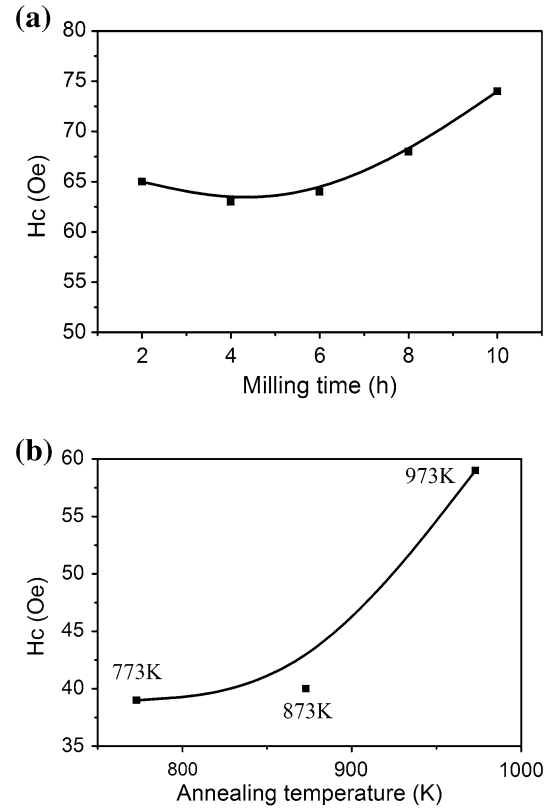

Fig. 6. H_c variations of the ball-milled $Fe_{65}Co_{35}$ powder mixture as a function of (a) milling time and (b) annealing temperature.

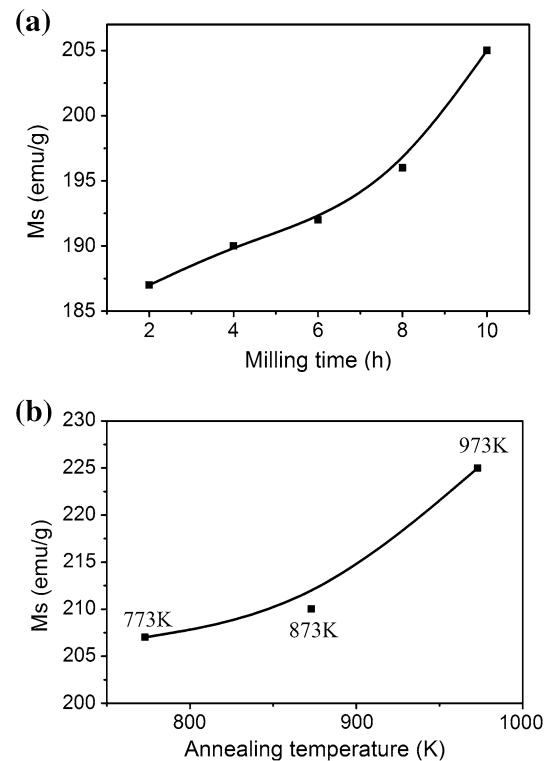

Fig. 7. Saturation magnetization dependence of $Fe_{65}Co_{35}$ powder mixture on (a) milling time and (b) annealing temperature at $T = 300$ K. Annealing time was 1 h.

Complementary Studies of Phase Formation During Fabrication of $Fe_{0.65}Co_{0.35}$ Nanoparticles by Mechanical Alloying

2507

oxidation and the surface/interface anisotropy effect.[7]

CONCLUSION

We have performed the complimentary studies on the phase formation during fabrication of $Fe_{0.65}Co_{0.35}$ nanoparticles by mechanical alloying in air and annealing by using both conventional XRD and synchrotron x-ray absorption spectroscopy techniques. The results have reconfirmed that the minor secondary phase of Fe_3O_4 could be detected from XRD experiments by choosing a very slow scanning rate to record the diffractogram. Meanwhile, XAS experiments show an oxidation state of +0 for the Fe ion, as well as the exact ratio of bcc and hcp structures in the samples that was expected. These results emphasize the unique sensitivity of these two complementary methods to follow the phase evolution and oxidation processes.

Magnetization measurements at room temperature indicated that M_s increased with milling times due to the alloying process, while the increase of M_s with annealing temperatures could be due to the reduction of oxidation, as well as the increase of particle size. The tendency of H_c to change depends not only on the annealing temperature, but also on the milling time (before annealing).

REFERENCES

1. N. Poudyal, C. Rong, Y. Zhang, D. Wang, M.J. Kramer, R.J. Hebertc, and J.P. Liu, *J. Alloys Compd.* 521, 55 (2012).
2. Y.X. Gong, L. Zhen, J.T. Jiang, C.Y. Xu, and W.Z. Shao, *J. Magn. Magn. Mater.* 321, 3702 (2009).
3. S.D. Bader, *Rev. Mod. Phys.* 78, 1 (2006).
4. A.H. Lu, E.L. Salabas, and F. Schuth, *Angew. Chem. Int. Ed.* 46, 1222 (2007).
5. Q.A. Pankhurst, J. Connolly, S.K. Jones, and J. Dobson, *J. Phys. D Appl. Phys.* 36, R167 (2003).
6. M. Abbas, M.N. Islam, B.P. Rao, T. Ogawa, M. Takahashi, and C.G. Kim, *Mat. Lett.* 91, 326 (2013).
7. Q. Zeng, I. Baker, V. McCreary, and Z. Yan, *J. Magn. Magn. Mater.* 318, 28 (2007).
8. A. Zelenakova, D. Oleksakova, J. Degmova, J. Kovac, P. Kollar, M. Kusy, and P. Sovak, *J. Magn. Magn. Mater.* 316, e519 (2007).
9. M. Sorescu and A. Grabias, *Intermetallics* 10, 317 (2002).
10. M. Hesani, A. Yazdani, B. Abedi Ravan, and M. Ghazanfari, *Sol. Stat. Commun.* 150, 594 (2010).
11. V. Mancier, J.L. Delplancke, J. Delwiche, M.J. Hubin-Franskin, C. Piquer, L. Rebbouh, and F. Grandjean, *J. Magn. Magn. Mater.* 281, 27 (2004).
12. Y.D. Kim, J.Y. Chung, J. Kim, and H. Jeon, *Mater. Sci. Eng., A* 291, 17 (2000).
13. D.K. Tung, D.H. Manh, P.T. Phong, L.T.H. Phong, N.V. Dai, D.N.H. Nam, and N.X. Phuc, *J. Alloys Compd.* 640, 34 (2015).
14. D.H. Manh, T.D. Thanh, N.X. Phuc, L.V. Hong, P.T. Phong, and L.T. Hung, *Int. J. Nanotechnol.* 8, 241 (2011).
15. P. Sirvent, E. Berganza, A.M. Aragón, A. Bollero, A. Moure, M. García-Hernández, P. Marín, J.F. Fernández, and A. Quesada, *J. Appl. Phys.* 115, 17B505 (2014).
16. D.H. Manh, D.K. Tung, D.N.H. Nam, L.V. Hong, P.T. Phong, N.X. Phuc, *I.E.E.E. Trans, Magn.* 50, 2005104 (2014).
17. D. Carta, G. Mountjoy, M. Gass, G. Navarra, M.F. Casula, and A. Corrias, *J. Chem. Phys.* 127, 204705 (2007).
18. S.N. Ehrlich, J.C. Hanson, A. LopezCamara, L. Barrio, M. Estrella, G. Zhou, R. Si, S. Khalid, and Q. Wang, *Nuc. Instr. Meth. Phys. Res. Sec A.* 649, 213 (2011).
19. B. Ravel and M. Newville, *J. Synchrotron Radiat.* 12, 537 (2005).
20. S. Azzaza, S. Alleg, H. Moumeni, A.R. Nemamcha, J.L. Rehspringer, and J.M. Greneche, *J. Phys.* 18, 7257 (2006).
21. D.-S. Yang, S.-H. Kim, Y.-G. Yoo, and S.-C. Yu, *J. Phys* 190, 012139 (2009).
22. G. Herzer, *IEEE Trans. Magn.* 26, 1397 (1990).
23. D.H. Manh, D.K. Tung, L.T.H. Phong, P.T. Thanh, and N.X. Phuc, *JPS Conf. Proc.* 1, 012010 (2014).
24. K. Akkouche, A. Guittoum, N. Boukherroub, and N. Souami, *J. Magn. Magn. Mater.* 323, 2542 (2011).